Polarization-insensitive silicon nitride photonic receiver at 1 μm for optical interconnects

Polarization-Insensitive Silicon Nitride Photonic Receiver at 1 μm for Optical Interconnects

Alexander Caut, Vijay Shekhawat, Victor Torres-Company, *Senior Member, Optica*, and Magnus Karlsson, *Fellow, Optica*

***Abstract*—This paper demonstrates with FDTD simulations a silicon nitride polarization independent coarse wavelength division multiplexing (CWDM) receiver platform based on square waveguides for optical interconnects at 1 μm. Here, the channel spacing of the demultiplexers is much smaller than standard CWDM systems (25 nm) and is set to 8 nm. To avoid high waveguide propagation and radiation losses, several waveguide dimensions were considered. The 450 nm (width) $\times$ 450 nm (height) waveguide presented a good tradeoff between low loss and single-mode behavior and was therefore selected. The demultiplexer has a simulated polarization dependence on the waveguide's width variations of 0.17 nm/nm. In addition, we present edge coupler designs with coupling loss within 2.5 dB for TE and TM polarization.**

***Index Terms*—Optical interconnects, silicon nitride, arrayed waveguide grating, Mach-Zehnder interferometer, coupling loss, polarization dependence, fiber misalignment, manufacturing tolerance.**

I. Introduction

POLARIZATION of the light propagating in a single mode fiber (SMF) cannot be controlled over distance and is therefore drifting randomly at the output of the SMF. Hence, integrated receivers need to be insensitive to polarization to avoid time-varying losses and high bit error rates (BERs). Such receivers based on silicon on insulator (SOI) have used the polarization diversity technique with a combination of splitters and rotators [1], [2]. The TM output port of the polarization splitter has an inserted rotator which rotates the electric field by 90°, converting the TM_{00} mode into a TE_{00} mode. The issue of this technique is the requirement for careful optimization of the designs to ensure a high polarization extinction ratio (PER) and polarization conversion efficiency (PEC) [1], [2]. Another approach, potentially simpler, is based on the use of square waveguides to directly achieve polarization independence. Hence, since the effective indices of the TE_{00} and TM_{00} modes are identical, the use of polarization splitters and/or rotators is not required. The coarse wavelength division multiplexing (CWDM) receiver in [3] was based on silicon nitride 600 nm $\times$ 600 nm waveguide. The demultiplexer was based on a cascaded Mach-Zehnder interferometer (MZI) and good polarization independence was demonstrated in the O-band. However, the issue with square waveguides is that roughness on the sidewalls can cause high propagation loss due to the strong interaction between the fundamental mode and the sidewalls of the waveguide. Indeed, the measured propagation loss in [3] was 190 dB/m. However, propagation losses close to 30 dB/m can still be achieved with square waveguides [4].

Future data centers will need to replace their abundant short-reach (<300 m) optical links based on GaAs vertical-cavity surface-emitting lasers (VCSELs) and multimode fibers (MMFs) at 850 nm. Indeed, these links, although inexpensive, are limited by modal dispersion and fiber attenuation. However, efficient single-mode GaAs-based VCSELs at 1060 nm have been demonstrated and could be modulated at 50 Gb/s using 4-pulse amplitude modulation [5], [6]. In addition, these VCSELs are more cost and energy efficient than standard InP distributed feedback (DFB) lasers at 1310 nm, used for longer links [7]. GaAs VCSELs at 1060 nm could be combined with SMFs for longer (>1 km) optical links, as a better alternative to links at 1310 nm using DFB lasers. To obtain high transmission speeds up to several Tb/s, coarse wavelength division multiplexing (CWDM) is being actively investigated for optical interconnects [6], [8], [9]. In our previous work, we mainly focused on the transmitter side and we demonstrated arrayed waveguide gratings (AWGs) and cascaded MZIs for CWDM at 1 μm [6], [8]. The channel spacing was set at 8 nm and the insertion loss of the multiplexers was within 2 dB. In addition, between silicon, silicon nitride, silica and other possible materials for our waveguide, we selected silicon nitride due to its good transparency at 1 μm and the good tradeoff it offers between compactness, fabrication tolerance and high mode confinement [8], [9], [10].

In this work, we focus on the receiver side. To the best of our knowledge, work on polarization independent receiver platforms at 1 μm is still missing. This paper proposes an analysis on the whole system in terms of simulated propagation loss and waveguide constraints on the polarization independence on each key component (demultiplexer and edge coupler). Polarization independent demultiplexers [3] and edge couplers [11] have been demonstrated. In addition, Daniel Y. Lee et al. demonstrated a polarization independent receiver at 1550 nm with micro ring resonators as a 4-channel demultiplexer [12]. However, work on numerical analysis on the receiver as a whole needs to be completed. In this work, we compare the simulated propagation loss

Manuscript received 30 November 2023; revised 26 March 2024; accepted 31 March 2024. Date of publication 3 April 2024; date of current version 18 April 2024. This work was supported in part by Swedish Research Council under Grant 2016-06077, and in part by iTRAN Project. *(Corresponding author: Alexander Caut.)*

The authors are with the Photonics Laboratory, Department of Microtechnology, Nanoscience, Chalmers University of Technology, SE-412 96 Göteborg, Sweden (e-mail: caut@chalmers.se).

Digital Object Identifier 10.1109/JPHOT.2024.3384870

of different waveguides and the impact of fabrication deviations on the polarization independence. Then, we demonstrate with simulations polarization independent edge couplers. Low loss edge couplers have been demonstrated with lensed SMFs. The drawbacks when using this type of fibers are the high cost due to the lenses and the increased difficulty to align the fiber with the edge coupler. In this work, we propose a solution with a standard SMF. The larger mode of the standard SMF will lead to higher coupling losses, but will also relax the difficulty to align with the edge coupler [11].

This paper is organized as follows: Section II goes through the platform considerations e.g. waveguide dimensions and the impact of fabrication deviations on the effective index. Section III then presents different edge couplers for the fiber-chip coupling where we consider a standard SMF instead of a lensed SMF. Finally, Section IV provides discussions followed by conclusions.

II. Platform Considerations

Several critical factors need to be considered for a polarization independent waveguide. The first parameter is the waveguide's dimensions and the second is the manufacturing tolerance. Our platform is based on a silicon nitride strip core surrounded by a cladding made of silica. The bottom SiO_2 cladding is deposited with a sputtering tool on top of a silicon substrate and is 4 μm-thick. For the Si_3N_4 layer deposition, low-pressure chemical vapor deposit (LPCVD) or plasma enhanced chemical vapor deposition (PECVD) deposition could potentially be used. While LPCVD deposition method offers the best material quality in terms of ultra-low loss applications in the IR range [13], its major drawback when the Si_3N_4 layer thickness exceeds 350 nm is that the material is prone to cracks due to high tensile stress [14]. This can be avoided by using the PECVD deposition method which offers less tensile stress and therefore a significant reduction in crack formations. However, this is at the cost of a lower material quality which would result in higher propagation loss. A good innovation which makes LPCVD Si_3N_4 still attractive for 350 nm thick layers is the use of crack barriers [15]. Moreover, thermal cycling the wafer also reduces the stress on the film, further reducing the cracks [16].

Since the waveguide has a square shape, the guided mode has a good confinement and the critical bending radius can be reduced, depending on the waveguide's dimensions. In addition, the core's size needs to be properly selected to obtain a single-mode behaviour since we want to avoid any excitation of side modes that could lead to additional loss or crosstalk.

The effective mode area and the critical bending radius of the guided TE_{00} and TM_{00} modes are calculated with Finite-Difference Eigenmode (FDE) simulations. The results are shown in Fig. 1(a) for different waveguide dimensions, with a dimension step of 50 nm^2. The vertical purple dashed line represents the waveguide's dimension threshold for multimode behaviour. It can be noticed the mode's effective area is at its minimum for a 450 $\times$ 450 nm^2 waveguide. Moreover, we simulated in Fig. 1(b) the propagation loss of these waveguides with the Payne Lacel model. The loss at the sidewalls, top and bottom of the waveguide are also plotted. In our simulations, we used root mean square (RMS) values and correlation lengths from [17]. The RMS values were 0.53 nm for the sidewall, 0.38 nm for the top and 0.284 nm for the bottom of the waveguide. Finally, the correlation length for the sidewalls, top and bottom are 47.4, 29 and 24 nm respectively. From the simulations, the total loss is at the highest (43.6 dB/m) for the 350 nm $\times$ 350 nm waveguide and drops down to 12 dB/m for the 800 nm $\times$ 800 nm multimode waveguide. For comparison, as we have an experimental scattering loss of 30 dB/m for a 900 nm (wide) $\times$ 160 nm (thick) Si_3N_4 waveguide at 1035 nm [6], we also simulated the scattering loss for this waveguide with the same RMS and correlation length and we found a loss of 33 dB/m, which is in excellent agreement with the experiments.

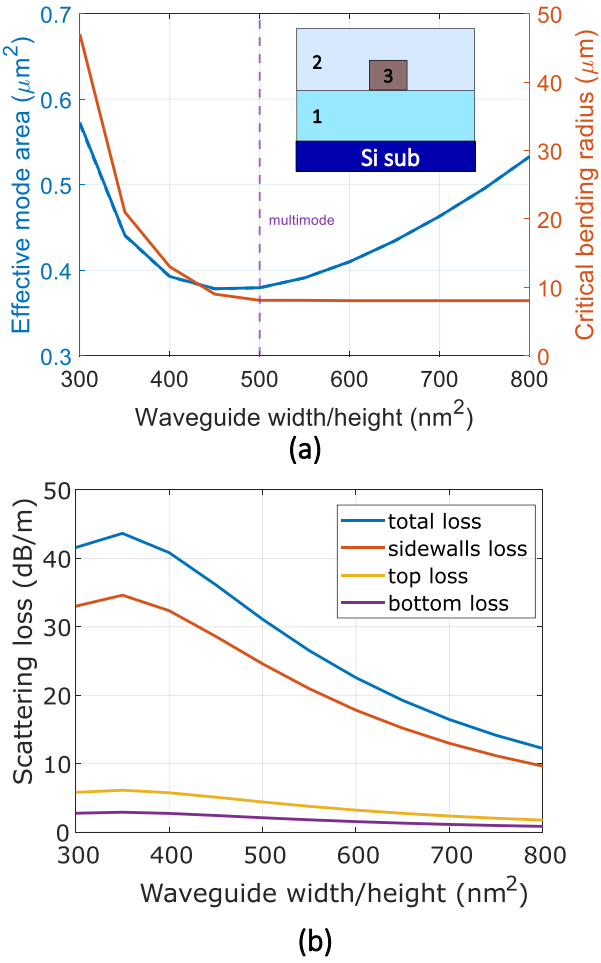

Fig. 1. (a) Effective area of the optical mode and critical bending radius for TE and TM polarization. The layers 1, 2 and 3 are respectively: thermal SiO_2, LPCVD SiO_2 and LPCVD (or PECVD) Si_3 N_4 (waveguide). The thermal and LPCVD layers are 4 μm-thick. (b) Scattering loss of the waveguide with the dimensions based on the Payne Lacel model.

Fig. 2 shows the electric fields of the TE_{00} mode for the 350 nm $\times$ 350 nm and the 450 nm $\times$ 450 nm waveguides. It can be noticed that the mode in the 350 nm $\times$ 350 nm waveguide has a stronger interaction with the sidewalls with respect to the mode in the 450 nm $\times$ 450 nm waveguide. This could explain the higher effective area for the first waveguide in Fig. 1 and the higher loss (43.6 dB/m vs 36.1 dB/m). In addition,

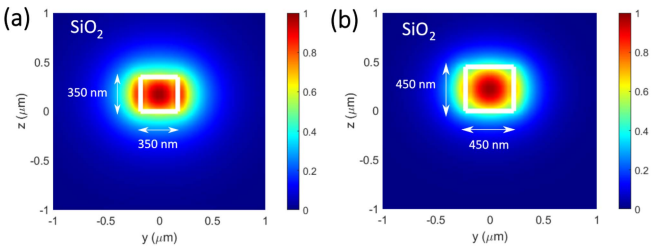

Fig. 2. Electric field amplitude of the TE_{00} mode for (a) the 350 nm × 350 nm and (b) the 450 nm × 450 nm waveguides.

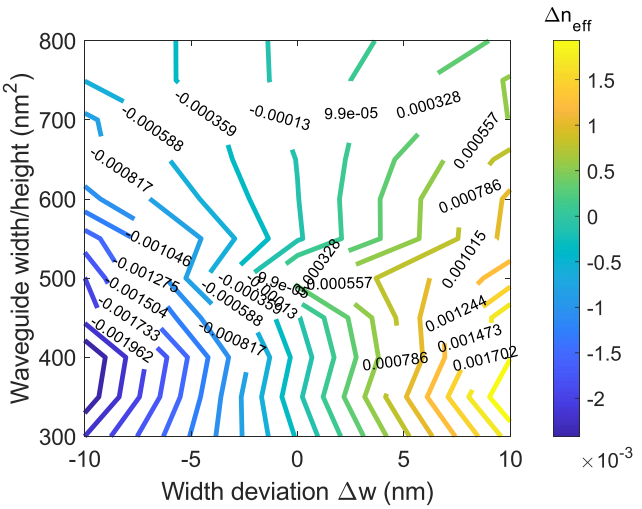

Fig. 3. Comparison of the effective index for TE and TM polarization when the width of the waveguide varies by ±10 nm from the target width. $\Delta n_{eff} = n_{eff,\,TE} - n_{eff,\,TM}$.

the FDE simulation results indicate negligible bending loss for waveguides larger than 450 nm × 450 nm (orange curve). Therefore, a 450 nm × 450 nm represents a good tradeoff between single-mode behaviour and strong confinement. The differential group delay between the TE_{00} and TM_{00} fundamental modes for the chosen waveguide's geometry was calculated with FDTD simulations. The estimated value was 4.37×10^{-5} ps/μm, which would become approximately 0.44 ps for a 1 cm-long waveguide in the photonic receiver.

Moreover, to estimate of the tolerance to fabrication deviations, we varied the width of the waveguide for several thicknesses and we calculated the difference between the effective indices of the TE and TM polarization. The results are plotted in Fig. 3 and indicate a value of $\Delta n_{eff} = -2.12 \times 10^{-3}$ for a 440 nm (width) × 450 nm (thickness) and 1.88×10^{-3} for a 460 nm (width) × 450 nm (thickness) waveguide. Such deviation in the waveguide geometry could thus translate into a polarization dependent receiver.

Regarding the demultiplexing (DEMUX) device, we considered the AWG and the cascaded MZI as potential candidates. These two components were compared in [8], [9] at 1060 nm. Silicon nitride was used as material for the waveguide in both cases and the waveguide dimensions were similar. The Gaussian AWGs demonstrated in [9] presented low insertion loss (within -1 dB) and low crosstalk (-35 dB). However, it was found in [8]

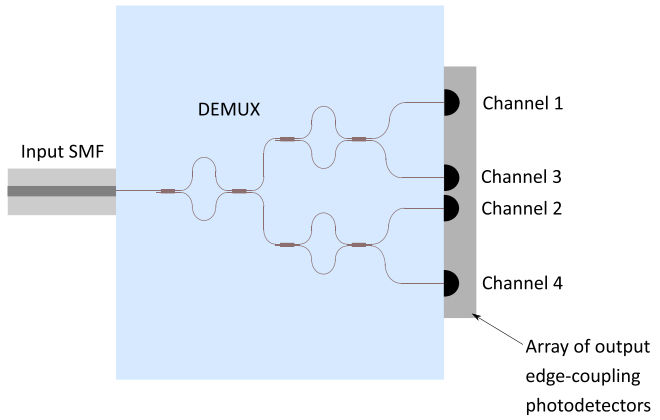

Fig. 4. Full receiver platform with input edge coupler.

that AWGs were more sensitive to manufacturing deviations such as improper etching and to tool calibration error than the cascaded MZI [8]. Therefore, the latter device was selected for this study. Cascaded MZIs use power splitters, which can be either based on directional couplers (DCs) or on multimode interferometers (MMIs). To reduce the crosstalk level [3], [9], we selected the MMI as the main power splitter due to its high tolerance to manufacturing deviations and low wavelength sensitivity [6].

The DEMUX is set as shown in Fig. 4. The input SMF is glued at the edge of the chip and an array of photodetectors is also attached at the other side of the DEMUX, where the the wavelengths are out-coupled. For our simulations, we considered a THORLABS HI1060-J9 SMF, operating from 980 nm to 1650 nm. The selected core diameter is 5.3 μm for a numerical aperture of 0.14 and the output mode field diameter is circa 6.2 μm at 1060 nm. To estimate the polarization dependence on variations of the waveguide dimensions, we simulated in Fig. 5 the impact of an imperfectly square waveguide on the spectral response of a cascaded MZI based on a 450 nm × 450 nm waveguide. The width was voluntarily reduced to 440 nm as we believe that a shift of 10 nm would be the worst case scenario. From the simulations, a shift of 1.7 nm between the TE and TM polarization was found. An additional shift of 2 nm towards shorter wavelengths can be observed. Therefore, in the worst case, a 10 nm width deviation in the waveguide would lead to an additional loss of 2.6 dB for the TE polarization and 0.6 dB for the TM polarization. Fig. 6 shows the simulated transmission of the MMI used in the cascaded MZI for the TE and TM polarization. Here, only the case when the waveguides are perfectly square is presented as the 440 nm × 450 nm waveguide did not have a significant impact on the device's performance. The results clearly show the small impact of the polarization on the device's performance as the simulated transmission is between -3.3 and -3.06 dB depending on the wavelength and the polarization.

III. Edge Taper Designs

For our receiver platform, edge and grating couplers were considered. Edge couplers have the advantage of high coupling

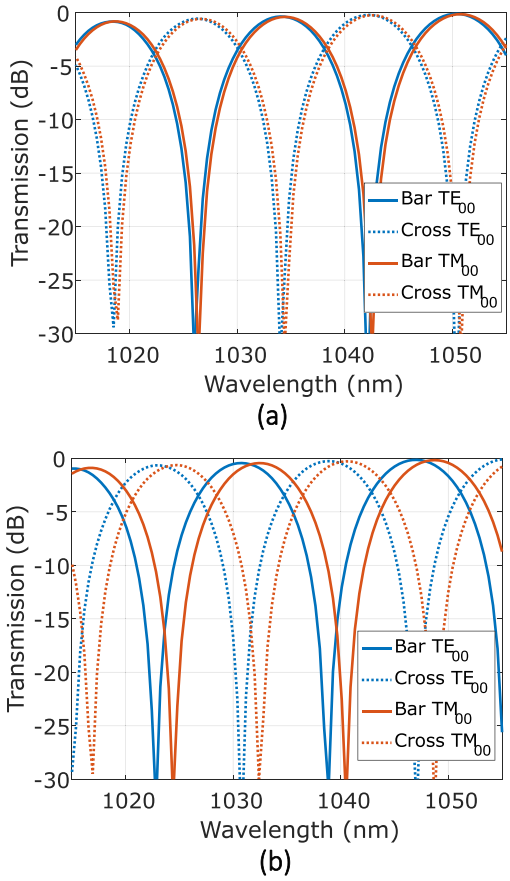

Fig. 5. Transmission of (a) the MZI filter for a perfectly square waveguide, (b) the MZI filter when the width of the waveguide is 440 nm. The blue and red curves represent the TE and TM polarizations respectively. The continuous and dashed curves stand for the bar and cross output of the MZI respectively.

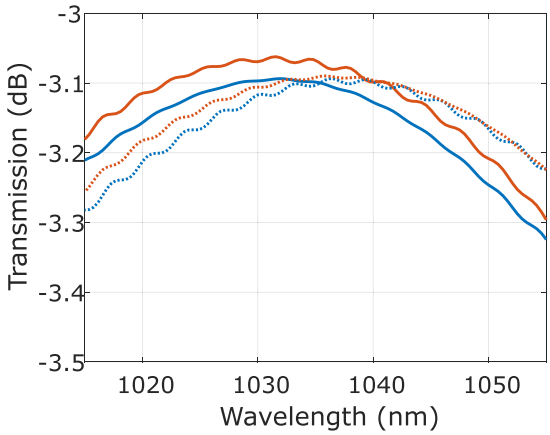

Fig. 6. Transmission of the MMI. The blue and orange lines correspond to the TE and TM mode respectively. The continous lines stand for the bar outputs and the dashed lines for the cross outputs of the device.

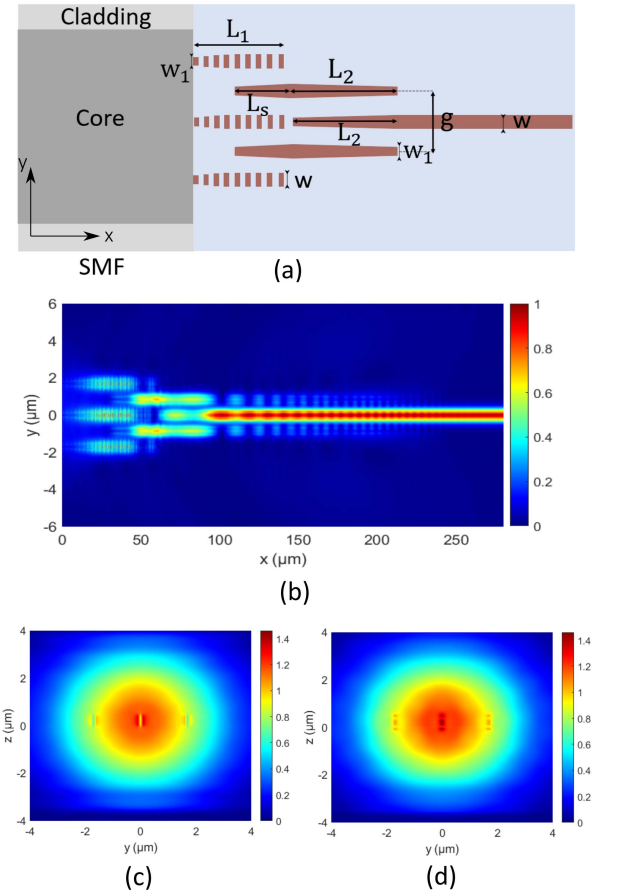

Fig. 7. (a) Main parameters of the grating assisted-trident: $L_1 = 60$ μm, $L_2 = 180$ μm, $L_s = 30$ μm, $w_1 = 100$ nm, $w = 450$ nm, $g = 1.7$ μm. The tip width of the central taper is 350 nm and the width of the side tapers is 400 nm. (b) Electric field amplitude of the device. Mode field profile at the chip facet for TE (c) and TM (d) polarization.

efficiency and of polarization tolerance [6], but they are also sensitive to fiber-chip misalignment. Grating couplers on the other hand are more tolerant to misalignment [18] but are also dependent on the fiber polarization [19]. The polarization dependence of grating couplers could be solved with the use of 2D-gratings [19], [20], [21] but high coupling efficiency grating couplers require careful apodization and a bottom reflector to reach values within -2 dB [20], [21]. Therefore, we considered the edge coupling approach with a trident design to reduce loss and polarization dependence. The proposed polarization independent edge coupler is based on a well-known design scheme which is a sub-wavelength grating trident. The design is first compared to a conventional taper and to a trident. Then we propose a study of the impact of a change of different parameters e.g. the gap between the side-tapers, the width and cladding thickness on the coupling loss and effective index of the coupled mode for TE and TM polarization.

In this section, the Si_3N_4 waveguide has a dimension of 450 nm $\times$ 450 nm and the thickness is kept the same for the tapers. With the optical fiber made of a silica waveguide and the photonic integrated circuit being made of Si_3N_4, this will result in a effective index difference between the fiber mode and the waveguide mode: 1.446 for the SMF and 1.665 for the 450 nm $\times$ 450 nm Si_3N_4 waveguide. This significant effective index difference causes reflection loss [11]. However, by tapering the waveguide at the chip's edge, it is possible to match the mode's effective index with that of

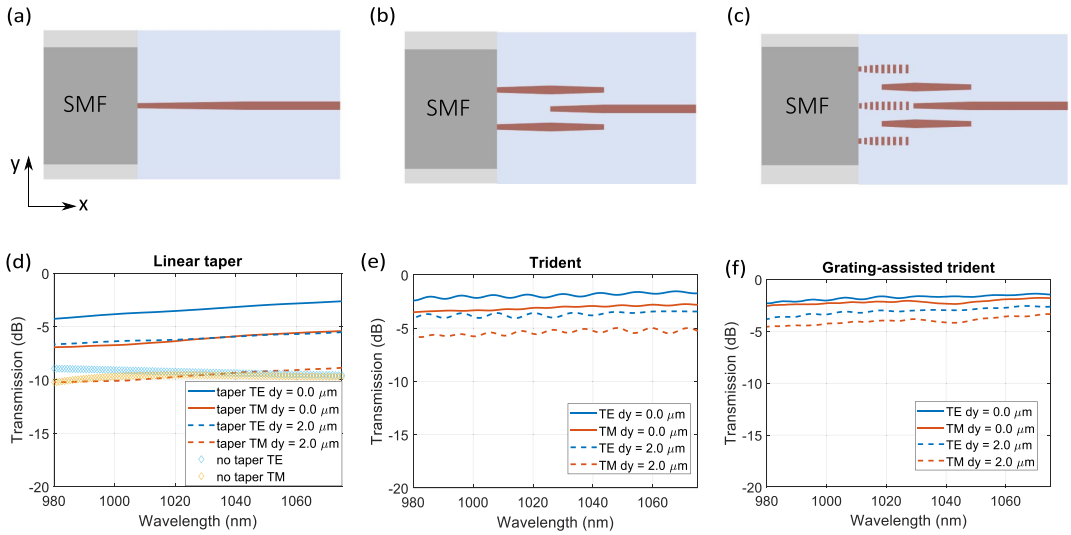

Fig. 8. Schemes of the considered designed (a) Linear taper (b) trident (c) grating assisted trident (d)–(f) Comparison of the transmission of the three edge taper designs for both TE and TM polarization.

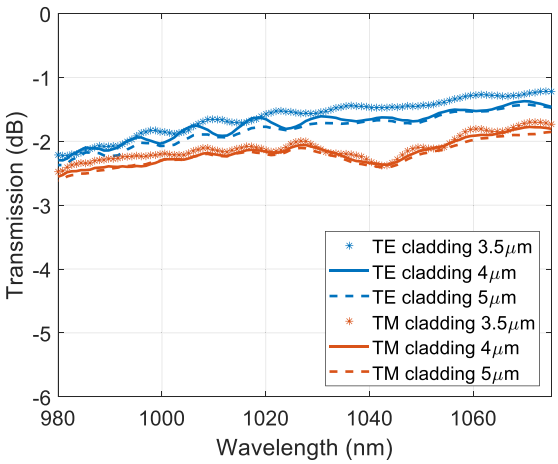

Fig. 9. Simulation of the grating trident taper for different cladding thicknesses.

the SMF and to therefore reduce the reflection loss. Nevertheless, the main contributing factor to the coupling loss is the mode mismatch between the SMF and the waveguide, which results in radiation and scattering loss [11]. Several techniques to reduce the mode mismatch and thus the coupling loss consist in multi-tips or multi-stages tapers [22]. The technique explored in this paper is the multi-tips technique. Fig. 7(a) shows a scheme of a trident design using subwavelength grating (SWG) tips. Similar designs using multi-tips with SWGs to improve the coupling efficiency have been demonstrated in [11], [23], [24]. With respect to conventional trident or forks designs, SWG tridents take advantage of the flexibility of the effective index which can be engineered by modifying the duty cycle of the grating. Fig. 7(b) shows the electric field distribution of the whole device. In addition, as it can be seen in Fig. 7(c) and (d), the SMF's mode is significantly larger than the Si_3N_4 waveguide's mode. The coupling efficiency of an edge taper is determined the modal overlap between the fiber mode and the coupled mode at the edge facet of the taper. The modal overlap is expressed

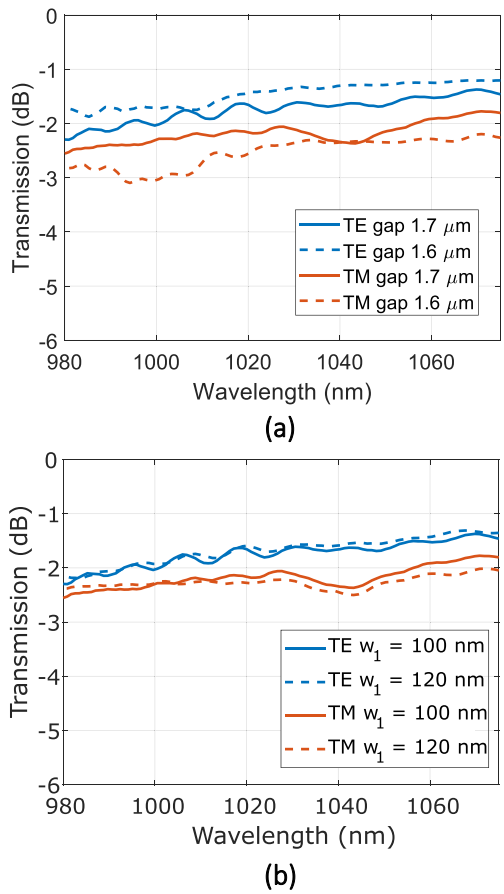

Fig. 10. Fabrication tolerance of the main parameters of the grating trident taper. (a) Transmission of the device for TE and TM polarization for gaps of 1.6 and 1.7 μm. (b) Transmission for different tip widths w_1 when the gap is 1.7 μm.

as [11], [18], [22]

$$\eta = \frac{|\int E_{SMF} E_{facet}{}^{*} dA|^2}{\int |E_{SMF}|^2 dA \int |E_{facet}|^2 dA} \quad (1)$$

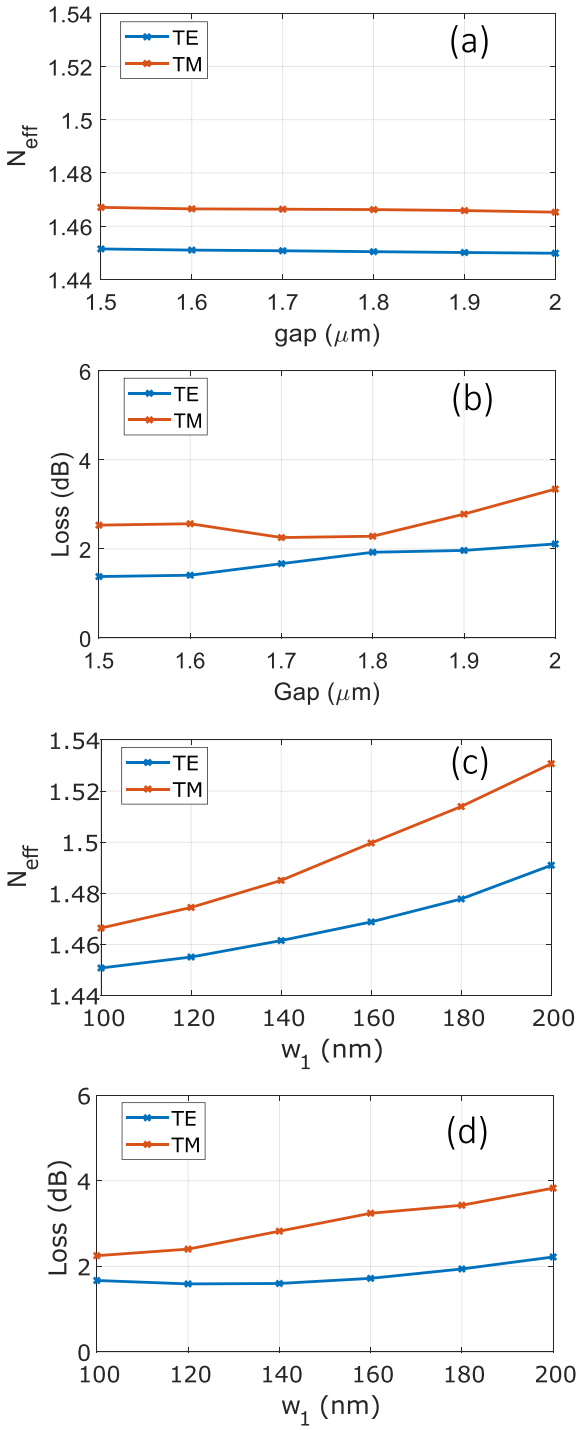

Fig. 11. Loss analysis of the device. (a) Effective index of the coupled mode at the edge of the chip for different gaps. (b) Loss at 1035 nm with the gap. (c) Effective index of the coupled mode at the edge of the chip for different tip widths w_1. (d) Loss at 1035 nm with the tip width w_1.

where E_{SMF} is the electrical field of the SMF, E_{facet} is the electrical field of the coupled mode at the edge facet of the taper and dA is the differential modal distribution area. Therefore, to obtain optimal coupling efficiency, the mode field at the chip facet and the SMF mode field should overlap completely, hence maximizing η.

Fig. 8 shows the different taper designs (linear, trident, grating assisted trident) with the input/output single mode fiber at the edge of the photonic integrated circuit (PIC). The gap between the side tapers for the trident designs in Fig. 8(b) and (c) is 1.7 μm. In addition, the grating-assisted trident design has 211 grating periods, where the grating period is 285 nm. The tip width of the central and side tapers are respectively 350 nm and 100 nm. We considered a SMF as illustrated in Fig. 8(a)–(c) with a core diameter of 5.3 μm. As the numerical aperture of the SMF was 0.14, we considered a refractive index of 1.45 for the core and 1.443 for the cladding. To avoid mode leakage into the substrate and to relax the misalignment tolerance between the fiber and the edge coupler, the selected thicknesses of the top and bottom cladding are 4 μm. Fig. 8(d), (e) and (f) presents the simulation results from a conventional linear edge taper, a trident taper and a trident taper assisted with gratings.

We considered a reference waveguide without taper at the edge of the chip for comparison with the considered edge couplers. Fig. 8(d) compares a 300 μm-long linear taper with a simple 300 μm-long waveguide. The edge coupler designs are long enough to obtain an adiabatic mode conversion from the SMF and the waveguide in the PIC. The reference waveguide has a coupling loss of 10 dB for both polarization due to the effective index mismatch between the SMF's mode and the waveguide's mode. The taper has a reduced coupling loss of 3.4 dB and 6 dB for TE and TM polarization respectively at 1030 nm. Due to the better confined TM_{00} mode in the 100 nm wide and 450 nm thick waveguide tip, the mode mismatch between the fiber and the waveguide is significantly higher for the TM polarization, which results in a higher coupling loss. The taper is also sensitive to lateral misalignment as a ± 2 μm deviation in the y-direction from the optimal spot results in a loss of 2.6 dB.

The trident taper (Fig. 8(e)) has a coupling loss of 2 dB for TE and 3 dB for TM polarization. When the SMF is shifted by 2 μm in the y-direction, the coupling loss becomes 3.8 dB for TE and 5.3 dB for TM. This design also presents an improved tolerance to fiber misalignment with respect to the linear taper. Indeed, the simulated additional loss for a ± 2 μm deviation in the y-direction is 1.8 dB.

The grating-assisted trident (Fig. 8(f)) proposes an interesting reduction in the polarization dependence of 0.5 dB. The coupling loss of the design is 1.7 dB and 2.2 dB for TE and TM polarization. In addition, the tolerance to fiber-chip misalignment is slightly further improved. The simulated additional loss for a ± 2 μm deviation in the y-direction is 1.3 dB.

In Fig. 9 we show the transmission of the subwavelength grating trident for different cladding thicknesses for the TE and TM polarization. Overall, when sufficiently thick, the top and bottom claddings have a relatively small impact on the device's transmission. A thickness of 3 μm was not considered in this case due to the large fiber mode size and to avoid mode leakage into the substrate.

We finally simulated the manufacturing tolerance of the grating-assisted trident by varying the distance between the side-tapers (and tapered-gratings) and the tip widths of the side tapers. Here, a cladding thickness of 4 μm was selected. In Fig. 10 are plotted the transmission of the device for different

gaps and tip widths w_1. The effective index of the coupled mode at the edge of the SWG trident and the coupling loss at 1035 nm are also plotted in Fig. 11. We can observe that any fabrication deviation in the design will have an impact not only on the insertion loss, but also in the polarization dependence. The gap is swept between 1.5 and 2.0 μm and has a relatively small impact on the effective index (Fig. 11(a)). However, it has an impact on the coupling loss as shown in Fig. 11(b). Indeed, the length L_s of the side-tapers was only optimized for a gap of 1.7 μm. Therefore, when the gap is changed, the lengths L_s is no longer optimized, creating destructive interferences. The width w_1 of the tips has a strong impact on the coupled mode's effective index as shown in Fig. 11(c). The resulting loss is higher for the TM polarization because the TM_{00} mode is better confined than the TE_{00} mode at the edge of the taper. Indeed, the taper is 450 nm thick and the width w_1 is only between 100 and 200 nm at the tip. Increasing the width of the taper leads to a faster increase of the effective index of the TM_{00} mode than for the TE_{00} mode as the plots show in Fig. 11(c). This leads to a larger mode mismatch with the SMF and thus, to a higher coupling loss in Fig. 11(d).

IV. Conclusion

We proposed a polarization independent integrated receiver based on a silicon nitride square waveguide. Among the possible dimensions, the 450 nm $\times$ 450 nm waveguide is a good tradeoff between single-mode behaviour, mode confinement and propagation loss. The simulated propagation loss is 36.1 dB/m for the chosen waveguide geometry. From our FDTD simulations, the demultiplexer has a spectral polarization dependence on the waveguide's width variations of 0.17 nm/nm. The bandwidth of the demultiplexer's channel is sufficiently large to compensate the spectral shift for the VCSEL signal to be detected regardless the polarization state. However, the crosstalk from the signals of the adjacent VCSELs would become more significant since the channel spacing is only 8 nm in this case.

We also proposed different designs of edge couplers and compared direct coupling to an untapered waveguide as a reference. The trident design shows a polarization dependence of 1 dB when the SMF is properly aligned. This difference increases up to 1.7 dB when the SMF is misaligned by 2 μm. The grating-assisted trident design however has a reduced polarization dependence between 0.5 and 0.7 dB. The loss of the device is within 2.2 dB for the TM polarization and has a bandwidth sufficiently large. In addition, the device has a decent tolerance to manufacturing deviations and is sufficiently compact for an edge coupler made of silicon nitride, which makes this design an interesting candidate. We also observe that the grating-assisted trident completely outperforms the simple linear taper in terms of loss, polarization independence and fiber-chip alignment. The most critical parameters of this design are the gap between the central and side tapers and the width of the tips, which have a strong impact on the loss and the polarization dependence. The loss could be further reduced with a more complex design involving several layers of silicon nitride waveguides, but would also increase the fabrication complexity [22].

References

[1] B. Troia et al., "Design and optimization of polarization splitting and rotating devices in silicon-on-insulator technology," *Adv. OptoElectronics*, vol. 2014, pp. 26–41, 2014.

[2] Y. Zhang et al., "Ultra-compact and highly efficient silicon polarization splitter and rotator," *APL Photon.*, vol. 1, 2016, Art. no. 091304.

[3] J. C. Mikkelsen, A. Bois, T. Lordello, D. Mahgerefteh, S. Menezo, and J. K. S. Poon, "Polarization-insensitive silicon nitride mach-zehnder lattice wavelength demultiplexers for CWDM in the O-band," *Opt. Exp.*, vol. 26, no. 23, pp. 30076–30084, 2018.

[4] M. Girardi, A. Larsson, and V. Torres-Company, "Performance tradeoffs in low-loss Si3N4 waveguides for linear and nonlinear applications," in *Proc. Eur. Conf. Integr. Opt.*, 2022, pp. 12–14.

[5] M. Jahed, J. S. Gustavsson, and A. Larsson, "VCSEL wavelength setting by intra-cavity phase tuning - numerical analysis and experimental verification," *IEEE J. Quantum Electron.*, vol. 57, no. 6, Dec. 2021, Art. no. 2400307.

[6] X. Hu, M. Girardi, Z. Ye, P. Muñoz, A. Larsson, and V. Torres-Company, "Si3N4 photonic integration platform at 1 μm for optical interconnect," *Opt. Exp.*, vol. 28, no. 9, pp. 13019–13031, 2020.

[7] A. Larsson et al., "1060 nm VCSELs for long-reach optical interconnects," *Elsevier Opt. Fiber Technol.*, vol. 44, pp. 36–42, 2018.

[8] A. Caut, M. Girardi, V. Torres-Company, A. Larsson, and M. Karlsson, "Channel scalability of silicon nitride (de-)multiplexers for optical interconnects at 1 μm," *J. Lightw. Technol.*, vol. 42, no. 1, pp. 276–286, Jan. 2024.

[9] S. S. Cheung and M. R. T. Tan, "Silicon nitride (Si3N4) (de-)multiplexers for 1-μm CWDM optical interconnects," *J. Lightw. Technol.*, vol. 38, no. 13, pp. 3404–3413, Jul. 2020.

[10] T. Akiyama et al., "Cascaded AMZ triplets: A class of demultiplexers having a monitor and control scheme enabling dense WDM on si nanowaveguide PICs with ultralow crosstalk and high spectral efficiency," *Opt. Exp.*, vol. 29, no. 6, pp.7966–7985, 2021.

[11] A. He, X. Guo, T. Wang, and Y. Su, "Ultracompact fiber-to-chip metamaterial edge coupler," *ACS Photon.*, vol. 8, no. 11, pp. 3226–3233,2021.

[12] D. Y. L. et al., "Error-free operation of a polarization-insensitive 4λ x 25 Gbps silicon photonic WDM receiver with closed-loop thermal stabilization of si microrings," *Opt. Exp.*, vol. 24, no. 12, pp. 13204–13209, 2016.

[13] W. D. Sacher, Y. Wang, G.-Q. Lo, and J. Poon, "Multilayer silicon nitride-on-silicon integrated photonic platforms and devices," *J. Lightw. Technol.*, vol. 33, no. 4, pp. 901–910, Feb. 2015.

[14] C. Yang and J. Pham, "Characteristic study of silicon nitride films deposited by LPCVD and PECVD," *Silicon*, vol. 10, no. 6, pp. 2561–2567, 2018.

[15] R. M. Grootes, M. Dijkstra, and Y. Klaver, "Crack barriers for thick sin using dicing," *Opt. Exp.*, vol. 30, no. 10, 2022, Art. no. 16725.

[16] A. Gondarenko, J. Levy, and M. Lipson, "High confinement micron-scale silicon nitride high Q ring resonator," *Opt. Exp.*, vol. 17, no. 14, pp. 11366–11370, 2009.

[17] S. Roberts, X. Ji, J. Cardenas, M. Corato-Zanarella, and M. Lipson, "Measurements and modeling of atomic-scale sidewall roughness and losses in integrated photonic devices," *Adv. Opt. Mater.*, vol. 10, no. 18, 2022, Art. no. 2102073.

[18] M. Jahed et al., "Angled flip-chip integration of VCSELs on silicon photonics integrated circuits," *J. Lightw. Technol.*, vol. 40, no. 15, pp. 5190–5200, Aug. 2022.

[19] F. V. Laere, W. Bogaerts, P. Dumon, G. Roelkens, D. V. Thourhout, and R. Baets, "Focusing polarization diversity grating couplers in silicon-on-insulator," *J. Lightw. Technol.*, vol. 27, no. 5, pp. 612–618,Mar. 2009.

[20] L. Cheng, S. Mao, Z. Li, Y. Han, and H. Y. Fu, "Grating couplers on silicon photonics: Design principles, emerging trends and practical issues," *MPDI Micromachines*, vol. 11, 2020, Art. no. 666.

[21] B. Chen et al., "Two-dimensional grating coupler on silicon with a high coupling efficiency and a low polarization-dependent loss," *Opt. Exp.*, vol. 28, no. 3, pp. 4001–4009, 2020.

[22] X. Mu, S. Wu, L. Cheng, and H. Fu, "Edge couplers in silicon photonic integrated circuits: A review," *MPDI: Appl. Sci.*, vol. 10, 2020,Art. no. 1538.

[23] A. He, X. Guo, K. Wang, Y. Zhang, and Y. Su, "Low loss, large bandwidth fiber-chip edge couplers based on silicon-on-insulator platform," *J. Lightw. Technol.*, vol. 38, no. 17, pp. 4780–4786,Sep. 2020.

[24] Y. Xiao, Y. Xu, Y. Dong, B. Zhang, and Y. Ni, "A 60 m-long fiber-to-chip edge coupler assisted by subwavelength grating structure with ultralow loss and large bandwidth," *MPDI: Photon.*, vol. 9, 2022,Art. no. 413.